ACS APPLIED MATERIALS & INTERFACES

www.acsami.org

Research Article

Effects of Cu Precursor on the Performance of Efficient CdTe Solar Cells

Sandip S. Bista,[§] Deng-Bing Li,[*,§] Rasha A. Awni, Zhaoning Song, Kamala K. Subedi, Niraj Shrestha, Suman Rijal, Sabin Neupane, Corey R. Grice, Adam B Phillips, Randy J. Ellingson, Michael Heben, Jian V. Li, and Yanfa Yan[*]

Cite This: *ACS Appl. Mater. Interfaces* 2021, 13, 38432−38440

Read Online

ACCESS | Metrics & More | Article Recommendations | Supporting Information

ABSTRACT: Copper (Cu) incorporation is a key process for fabricating efficient CdTe-based thin-film solar cells and has been used in CdTe-based solar cell module manufacturing. Here, we investigate the effects of different Cu precursors on the performance of CdTe-based thin-film solar cells by incorporating Cu using a metallic Cu source (evaporated Cu) and ionic Cu sources (solution-processed cuprous chloride (CuCl) and copper chloride ($CuCl_2$)). We find that ionic Cu precursors offer much better control in Cu diffusion than the metallic Cu precursor, producing better front junction quality, lower back-barrier heights, and better bulk defect property. Finally, outperforming power conversion efficiencies of 17.2 and 17.5% are obtained for devices with cadmium sulfide and zinc magnesium oxide as the front window layers, respectively, which are among the highest reported CdTe solar cells efficiencies. Our results suggest that an ionic Cu precursor is preferred as the dopant to fabricate efficient CdTe thin-film solar cells and modules.

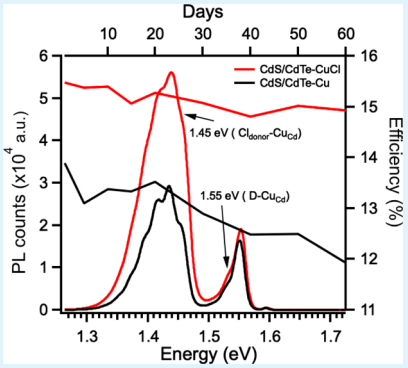

KEYWORDS: *CdTe solar cell, CuCl, $CuCl_2$, ionic Cu precursor, Cu doping*

INTRODUCTION

Cadmium telluride (CdTe) solar cell technology has been attracting extensive attention due to its low cost and ideal band gap for high-efficiency photovoltaics.[1] First solar, limited liability company (LLC) has reported the highest power conversion efficiencies (PCEs) of 22.1% for small area cells and 19% for modules, providing a competitive alternative for traditional silicon photovoltaics.[2] For most efficient CdTe solar cells and modules, copper (Cu) is applied as a dopant to improve the p-type conductivity of the CdTe absorber and to reduce the Schottky barrier height between the CdTe and the back contact.[3−6] The Cu incorporation is typically done via the post-deposition of a thin layer of Cu source material on $CdCl_2$-treated CdTe thin films. The Cu concentration (N_{Cu}) and distribution in the CdTe absorber layer can significantly influence the performance of CdTe solar cells.[7] For example, excessive Cu incorporation can introduce interstitial defects (Cu_i) and other Cu related compensation complexes, e.g., Cu_i-Cu_{Cd},[8] which would limit the hole density in CdTe films. Additionally, Cu_i ions can diffuse at a high speed due to its high solubility at grain boundaries,[9−12] which adversely affects the long-term stability of CdTe solar cells.[13−15] More importantly, Cu at the front interfaces (e.g., the cadmium sulfide (CdS)-CdTe and zinc magnesium oxide (ZMO)-CdTe interfaces) has been thought to form recombination centers and shunting pathways, leading to the degradation of device performance.[3,16] Therefore, the Cu dosage and distribution in CdTe films should be well controlled to minimize the nonradiative recombination related to Cu doping and maximize the device performance and long-term stability.

In this regard, various Cu precursors have been used as the Cu source to fabricate CdTe thin-film solar cells. In general, two kinds of Cu precursors, including metallic Cu,[17] covalent Cu compounds, e.g., Cu_xTe,[18] Cu doped ZnTe,[19] and ionic Cu compounds, e.g., CuSCN,[20,21] cuprous chloride (CuCl),[3,5,6] and copper chloride ($CuCl_2$).[22,23] Among them, CuCl and $CuCl_2$ have attracted extensive attention due to its outstanding performance. Recently, $CuCl_2$ was incorporated in the CdTe absorber as the Cu precursor to eliminate the diffusion of Cu into the front junction, achieving a maximum PCE of ∼16%.[22] Sites and coworkers have demonstrated a record PCE of 19.1% for CdSeTe solar cells using the CuCl precursor deposited by close space sublimation (CSS).[5,24] We previously reported a PCE of 17.5% for CdTe solar cells (no selenium) using a solution-processed CuCl treatment with rapid thermal anneal-

Received: June 23, 2021
Accepted: July 23, 2021
Published: August 4, 2021

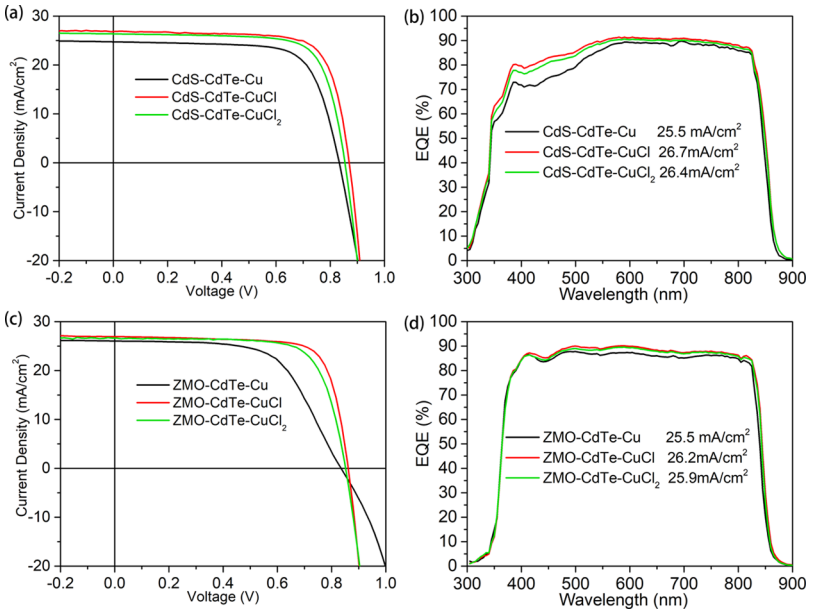

Figure 1. (a, c) *J*−*V* curves and (b, d) EQE spectra of representative (a, b) CdS-CdTe and (c, d) ZMO-CdTe devices treated with different Cu precursors.

ing process.[3] However, to date, comparative investigations on the impact of Cu precursors have rarely been reported.

Here, we report on a comparative study of the effects of Cu precursors on the performance of CdTe-based thin-film solar cells. Please note that no etching treatment is performed on the chlorinated CdTe film in this work. We fabricate CdTe thin film solar cells using a metallic Cu source (evaporated Cu) and ionic Cu sources (solution-processed CuCl and $CuCl_2$). We find that the ionic Cu precursors offer much better control of Cu diffusion than the metallic Cu precursor. The statistical analysis of a large number of CdTe solar cells shows that the cells fabricated using the ionic Cu source show better front junction quality, lower back barrier heights, and better bulk defect property than the cells fabricated using the metallic Cu source. CuCl and $CuCl_2$, with different oxidation states of Cu, deliver almost the same performance for CdTe solar cells, which are much better than the cells that with the metallic Cu source. Our results show that the ionic Cu precursor plays a critical role in controlling the Cu dosage and establishing a desired Cu distribution profile.

EXPERIMENTAL SECTION

CdTe solar cells with two kinds of electron transport layers, i.e., CdS and ZMO, were fabricated. For the CdS-CdTe devices, fluorine-doped tin oxide (FTO) coated glass (TEC 12D; NSG, US) with a 30 nm intrinsic SnO_2 layer was used as the substrate. First, an oxygenated cadmium sulfide (CdS:O) window layer with a thickness of 60 nm was deposited by radio-frequency (RF) magnetic sputtering using a 2-in. CdS target in a 2% oxygen and 98% argon environment at room temperature under 10 mTorr pressure and 50 W power. A 4-μm CdTe absorber was deposited by close-space sublimation (CSS) at the source and substrate temperatures of 660 and 590 °C, respectively, at 10 Torr pressure, followed by a wet cadmium chloride ($CdCl_2$) treatment at 390 °C for 30 min in dry air.[25]

For the ZMO-CdTe devices, FTO-coated glass (TEC 12; NSG, US) was used as the substrate according to our previous work.[3] A 80 nm ZMO window layer was deposited using a commercial ZMO target (8 wt % MgO) by RF sputtering with a flow gas of 16 sccm of pure argon and 24 sccm mixture gas of 95% argon and 5% oxygen. After a 10 min UV-ozone treatment for the as-deposited ZMO window layer, a 3.5 μm CdTe film was deposited by CSS with a source temperature of 560 °C and a substrate temperature of 495 °C under 1 Torr. Then, a $CdCl_2$ treatment was carried out at 420 °C for 20 min with a helium (He) flow (500 sccm) at 500 Torr.

After $CdCl_2$ treatment, the samples were rinsed with methanol to remove the residual $CdCl_2$ from the back surface. Then, three different Cu precursors were used to incorporate Cu for both CdS-CdTe and ZMO-CdTe devices. It is noted that no etching treatment was performed after $CdCl_2$ treatment for all the devices. The first Cu precursor was metallic Cu: a bilayer electrode of Cu (4 nm for CdS-CdTe and 3 nm for ZMO-CdTe devices) and Au (40 nm) was deposited by thermal evaporation with an individual cell area of 0.08 cm^2 followed by an activation treatment at 200 °C for 20 min. The second precursor was CuCl: a saturated CuCl (100 μL for CdS-CdTe and 80 μL for ZMO-CdTe devices) solution in ethanol was used to drop and spread on a 1.5″ × 1.5″ CdTe surface. After drying naturally, the samples were treated through rapid thermal annealing (RTA) (at 200 °C for CdS-CdTe and 160 °C for ZMO-CdTe devices) with a ramping speed of ∼60 °C/min without dwelling time in a 500 sccm He flow. The third precursor was $CuCl_2$: a $CuCl_2$ solution (with a Cu concentration of 3.10 μg/mL, 100 μL for CdS-CdTe and 80 μL for ZMO-CdTe devices) solution in ethanol was used to drop and spread on a 1.5″ × 1.5″ CdTe surface. After drying naturally, the samples were treated through RTA (at 200 °C for CdS-CdTe and 160 °C for ZMO-CdTe devices) with a ramping speed of ∼60 °C/min without dwelling time in a 500 sccm He flow. Note that the Cu ion concentration in both CuCl and $CuCl_2$ solution was 3.10 μg/mL. After the Cu activation annealing treatment, a 40 nm Au layer was deposited on the back surface with an individual device area of 0.08 cm^2. No further annealing treatment was taken after the Au deposition. Finally, a 120 nm magnesium fluoride (MgF_2) anti-reflective layer was deposited on the glass side of the FTO substrate in an e-beam evaporation system.

Hall effect measurements were performed for our as-deposited, $CdCl_2$-treated, and CuCl-treated CdTe films (∼3 μm) deposited on soda lime glass using a M91Fast Hall measurement system (LakeShore Cryotronics Advancing Science). All the as-deposited, $CdCl_2$-treated, and CuCl-treated CdTe films show p-type conductivity with hole concentrations in the order of 10^{12}, 10^{12}, and 10^{13} cm^{-3}, respectively. Solar cell performance was characterized by measuring current density−voltage (*J*−*V*) curves under AM1.5G illumination using a solar simulator and a source meter (Keithley 2400) and the external quantum efficiency (EQE) spectra using an EQE system (PV Measurements Inc.). Dynamic secondary ion mass spectrometry (SIMS) was performed using Dynamic-SIMS5 from ION-TOF

https://doi.org/10.1021/acsami.1c11784
ACS Appl. Mater. Interfaces 2021, 13, 38432−38440

Table 1. Photovoltaic Parameters for the Best CdS-CdTe and ZMO-CdTe Devices with Different Precursors

samples	V_{OC} (V)	J_{SC} (mA/cm^2)	FF (%)	PCE (%)	R_S (Ω cm^2)	R_{SH} (Ω cm^2)
CdS-CdTe-Cu	0.833	25.5	71.7	15.2	3.8	1140
CdS-CdTe-CuCl	0.870	26.4	75.1	17.2	1.7	1421
CdS-CdTe-$CuCl_2$	0.854	26.3	74.3	16.7	2.1	1209
ZMO-CdTe-Cu	0.837	25.9	61.8	13.4	9.8	1297
ZMO-CdTe-CuCl	0.862	26.9	75.5	17.5	1.7	1455
ZMO-CdTe-$CuCl_2$	0.851	26.6	73.3	16.7	2.6	1548

GmbH (Munster, Germany). The samples were analyzed in dual-beam profiling mode and the primary ion for analysis was 30 keV Bi^{3+} (Bi liquid metal ion source). This ion beam was applied over a 100 μm × 100 μm area at the center of the sputter crater (400 μm × 400 μm). The spectral data was acquired in high mass-resolution mode. The energy of the sputtered ion was 1 keV Ar^+ (Ar, electron impact ion source). Room-temperature capacitance−voltage ($C-V$), temperature-dependent current−voltage ($J-V-T$), thermal admittance spectroscopy (TAS), and impedance spectroscopy (IS) measurements were performed using a Solartron Modulab potentiostat equipped with a frequency response analyzer (Ametek Inc.). Photoluminescence (PL) characteristics were investigated utilizing steady-state and time-resolved PL. The detail of the electrical characterizations and PL measurement can be found in our previous publication.[3]

RESULTS

The representative device performance of CdTe solar cells with different Cu precursors (i.e., metallic Cu, CuCl, and $CuCl_2$, named CdTe-Cu, CdTe-CuCl, and CdTe-$CuCl_2$ hereafter, respectively) is shown in Figure 1. A detailed statistical comparison of all the photovoltaic parameters for the CdS-CdTe and ZMO-CdTe devices is shown in Figures S1 and S2, respectively. The best $J-V$ parameters for each type of device are tabulated in Table 1. For the devices with CdS as the front window layer (Figure 1a,b), the best CdTe-Cu device shows a PCE of 15.20%, with a V_{OC} of 833 mV, J_{SC} of 25.5 mA/cm^2, and FF of 71.7%, while the CdTe-CuCl device demonstrates an overall improved performance with a V_{OC} of 870 mV, J_{SC} of 26.4 mA/cm^2, and FF of 75.1%, yielding a PCE of 17.2%. The CdTe-$CuCl_2$ device exhibits a similar performance to the CdTe-CuCl device with a V_{OC} of 854 mV, J_{SC} of 26.3 mA/cm^2, and FF of 74.3%, yielding a PCE of 16.7%. When comparing the EQE results, the CdS-CdTe-CuCl and CdS-CdTe-$CuCl_2$ devices show a significantly increased spectral response in the wavelength range from 350 to 550 nm with respect to the CdS-CdTe-Cu device (Figure 1b) and deliver integrated current densities of 26.7 and 26.4 mA/cm^2, respectively, higher than that in the CdS-CdTe-Cu device (25.5 mA/cm^2). The significant improvement of EQE in the whole wavelength range for the CuCl- and $CuCl_2$-treated devices suggests better carrier separation and transport properties, especially at the front interface. This can be attributed to the reduced Cu diffusion to the front junction, which will be discussed later.

The performance of ZMO-CdTe solar cells with CuCl and $CuCl_2$ (Figure 1c) is also significantly improved compared with that of the metallic Cu-treated device (Figure 1c). The devices treated with solution-processed CuCl and $CuCl_2$ show higher quantum efficiencies of ∼90% from 500 to 600 nm, yielding an integrated current of 26.2 and 25.9 mA/cm^2, respectively, which are higher than the J_{SC} of 25.5 mA/cm^2 in the ZMO-CdTe-Cu device (Figure 1b). The statistical comparison in Figures S1 and S2 also show the same improvements for the devices with the CdS and ZMO front window layers, especially the V_{OC} and FF, suggesting a better front main junction and a reduced back barrier height. Interestingly, the J_{SC} values in the CdS-CdTe devices are higher than those in the ZMO-CdTe devices although ZMO has a larger band gap than CdS. One reason is that the CdS film in this work is thinner (60 nm) than the ZMO film (80 nm), resulting in higher transmittance at the range of 300−380 nm (Figure S3). The other reason is the interdiffusion between CdS and CdTe at the front interface, resulting in the formation of CdSTe alloy, which has a slightly smaller band gap.[26] Therefore, the light absorption of the CdS-CdTe device extended to longer wavelengths at the range of 840−880 nm as shown in the EQE curves (Figure S3). Please note that the etching treatment after $CdCl_2$ treatment is excluded due to its incompatibility with the ZMO-CdTe devices. Nonetheless, both metallic Cu and CuCl treatment are also applied on the CdS-CdTe device with and without hydroiodic (HI) acid etching treatment according to our previous procedure.[17] The results (Figure S4) further demonstrate that CdTe devices with CuCl treatment show better performance than those with metallic Cu treatment.

Note that the $J-V$ curves of the ZMO-CdTe device with Cu metal (Figure 1c) show clear distortion under a forward bias near V_{OC} (i.e., an S-kink), indicating poor heterojunction properties at the ZMO-CdTe interface. According to our SCAPS simulation results,[27] the S-kink can be attributed to the low ZMO film conductivity and the high acceptor-like defect trap concentration at the front interface, both of which are caused by the over diffusion of Cu. The diffusion of Cu into the ZMO film and the ZMO-CdTe interface can significantly decrease the ZMO conductivity[28−30] and form recombination centers at the front interface.[3,16] The aggregation of Cu at the front interface and in the ZMO layer is identified by the dynamic-SIMS measurements (Figure S5). Note that in the CdTe-CuCl devices, the Cu activation can be performed by an RTA process at 160 °C with ∼150 times less Cu dosage than the treatment using metallic Cu, as reported in our previous work.[3] The RTA process has also been tried for the devices with metallic Cu doping. However, the traditional Cu activation process (200 °C for 20 min) always shows higher device performance than that treated with the RTA process when metallic Cu is used as the Cu source (Figure S6). In comparison, the CdS-CdTe devices treated with metallic Cu show no S-kink. This is probably because CdS is not as sensitive to Cu as ZMO.

To further investigate the effect of different Cu precursors on the optoelectronic properties of CdTe films, a suite of characterizations was performed. Note that the CdTe-CuCl devices show similar performances to the CdTe-$CuCl_2$ devices, implying the nonessential effect of the oxidation state of ionic Cu. The slightly lower performance of the CdTe-$CuCl_2$ devices than the CdTe-CuCl devices may be attributed to experimental deviation and the film inhomogeneity. However, the devices treated with metallic Cu show much lower device performance than those with the solution processed CuCl and $CuCl_2$ treatments, suggesting a more significant effect of the ionic

https://doi.org/10.1021/acsami.1c11784
ACS Appl. Mater. Interfaces 2021, 13, 38432−38440

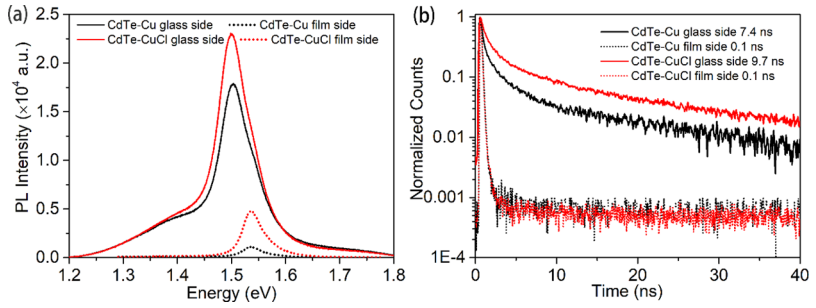

Figure 2. (a) PL and (b) TRPL spectra for CdTe-Cu and CdTe-CuCl devices with CdS as the front window layer. For each sample, PL spectra were excited through the FTO glass side and CdTe film side with a 633 nm laser excitation.

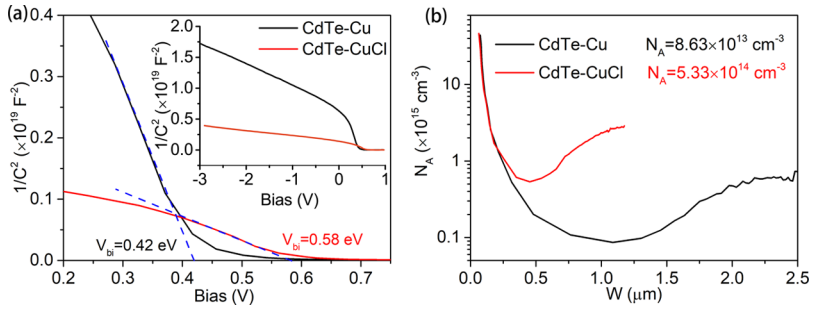

Figure 3. (a) Mott−Schottky plots measured at room temperature for devices with Cu and CuCl treatment. Inset: Mott−Schottky plots measured from −3.0 to 1.0 V bias voltage. (b) Calculated carrier densities extracted from *C*−*V* measurements.

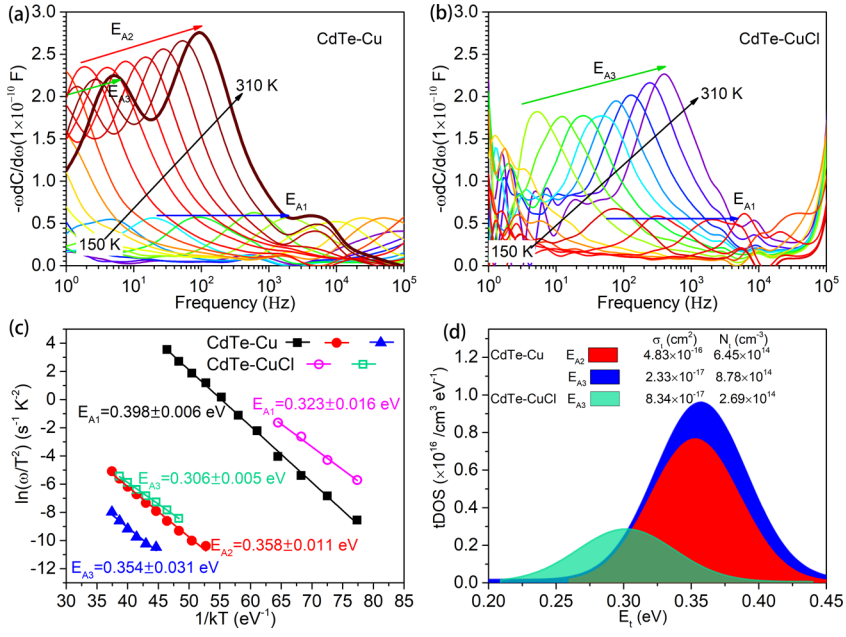

Figure 4. Differential capacitance spectra ($-\omega dC/d\omega$) extracted from the capacitance spectra in Figure S9 for (a) CdTe-Cu and (b) CdTe-CuCl devices. (c) Arrhenius plots and (d) defect distribution in CdTe-Cu and CdTe-CuCl devices obtained from (a) and (b). The trap defect activation energies (E_A), defect capture cross section (σ_t), and trap state densities (N_t) are tabulated in the inset.

versus metallic Cu sources. In addition, changing the front window layer, e.g., CdS and ZMO, does not affect the influence of different Cu precursors. Therefore, CdS-CdTe-CuCl was chosen as the representative of ionic Cu treatment to make comparison with the devices with metallic Cu in the characterization hereafter.

Figure 2a shows the PL measurements of CdTe-Cu and CdTe-CuCl devices with CdS as the front window layer. Both samples show PL spectra with an emission peak centered at 1.501 ± 0.003 eV when excited through the FTO glass side and 1.537 ± 0.002 eV when excited from the film side but with different emission intensities. The variation of the emission peaks is due to the interdiffusion of CdS and CdTe at the front interface.[31] Higher PL intensity generally suggests a lower nonradiative recombination rate and a higher carrier lifetime. For both glass and film side excitations, the CdTe-CuCl device shows higher PL intensities than the CdTe-Cu device, indicating lower recombination rates at the CdS-CdTe and CdTe-Au

https://doi.org/10.1021/acsami.1c11784
ACS Appl. Mater. Interfaces 2021, 13, 38432−38440

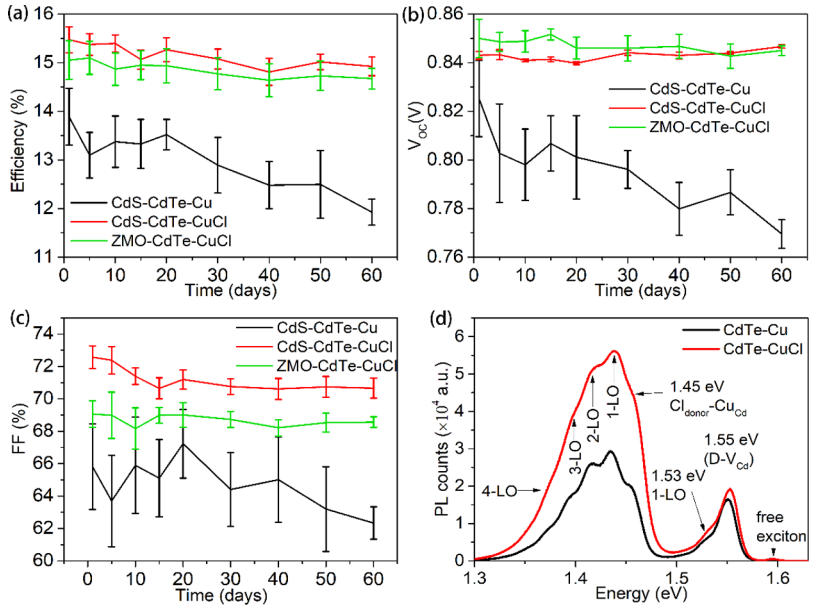

Figure 5. Degradation tests in ambient air for 60 days for devices with different window layers and Cu precursors. Each group includes 6 cells. The degradation of the (a) efficiency, (b) V_{OC}, and (c) FF was plotted individually. (d) Low-temperature steady-state PL measurement of CdTe-Cu and CdTe-CuCl devices excited from the back side at 9 K performed with a 532 nm laser at 25 mW/cm^2.

interfaces in the CdTe-CuCl device.[27] The TRPL results in Figure 2b further confirm this conclusion by showing a much higher carrier lifetime of 9.7 ns in the CdTe-CuCl device than that of 7.4 ns in the CdTe-Cu device when excited from the glass side. When excited from the film side, same lifetime is obtained due to the severe recombination at the back surfaces and the equipment detection limit. The same PL and TRPL measurements were also carried out for ZMO-CdTe devices, and similar trends can be observed with higher PL intensity and lifetime in the ZMO-CdTe films, as shown in Figure S7.

$C-V$ measurement was used to investigate the apparent build-in potential (V_{bi}) at the front junction and extract the doping density in the CdTe absorber layer (Figure 3a). From the intercept of the linear fit of the Mott−Schottky plot ($1/C^2$ vs bias) with the bias axis, the V_{bi} across the depletion region formed by the CdS-CdTe junction was extracted. The CdTe-CuCl device shows a higher V_{bi} (0.58 V) than the CdTe-Cu device (0.42 V) (Figure 3a). The improvement of V_{bi} suggests an improved front junction at the CdS and CdTe interface of the CdTe-CuCl device, which plays the most important role in V_{OC} and final device performance. The improvement of V_{bi} in the CdTe-CuCl device can be attributed to the improvement of hole density in the bulk CdTe absorber, the reduction of the interface trap state concentration, and higher n-type conductivity of the CdS film due to well-controlled Cu diffusion into the front interface and CdS film.[32] The apparent hole density N_A in the CdTe layer is calculated using the Mott−Schottky plot according to the following equation:[17]

$$N_A = -\frac{2}{q\varepsilon\varepsilon_0 A^2}\left[\frac{dC^{-2}(V)}{dV}\right]^{-1} \quad (1)$$

where ε is the relative dielectric constant of CdTe, ε_0 is the absolute permittivity of vacuum, A is the surface area of a cell, C is the junction capacitance, and V is the bias voltage. As shown in Figure 3b, the hole carrier concentration taken from the lowest point of its depth profile of the CdTe-CuCl device is 5.33×10^{14} cm^{-3}, which is higher than the carrier concentration in the CdTe-Cu device (8.63×10^{13} cm^{-3}). $C-V$ measurements for the ZMO-CdTe devices with varied Cu precursors were also performed and similar changes of the carrier concentration can be observed (Figure S8). The improvement of hole density in the CdTe bulk is beneficial to the improvement of V_{bi} as discussed above and the reduction of the back-barrier height, which will be discussed later.

Thermal admittance spectroscopy is an effective method to study the defect properties in CdTe solar cells.[17,33] The capacitance spectra ($C-\omega$) measured at various temperatures (T) for CdTe-Cu and CdTe-CuCl devices are shown in Figure S9. From the peaks of the derivative of capacitance spectra ($-\omega dC/d\omega$), Figure 4a,b, the defect characteristic frequencies as indicated by arrows were extracted and used to build the Arrhenius plots (Figure 4c). From the linear fit of the Arrhenius plots, the trap defect states in the CdTe-Cu and CdTe-CuCl devices were calculated. Here, three characteristic activation energies, $E_{A1} = 0.398 \pm 0.006$ eV, $E_{A2} = 0.358 \pm 0.011$ eV, and $E_{A3} = 0.354 \pm 0.031$ eV, for CdTe-Cu devices and two activation energies, $E_{A1} = 0.323 \pm 0.016$ eV and $E_{A3} = 0.306 \pm 0.005$ eV, for CdTe-CuCl devices were detected. According to our previous investigation about the TAS measurements performed at various DC biases with constant AC modulation,[17] E_{A1} corresponds to the back contact barrier, while E_{A2} and E_{A3} are considered as deep acceptor-like trap states.[17,34,35] For the CdTe-Cu device, a back-barrier height of 0.398 ± 0.006 eV is obtained, which is higher than the 0.323 ± 0.016 eV obtained in the CdTe-CuCl devices. This can be further demonstrated by the $J-V-T$ measurements as shown in Figure S10. The reduction of the back-barrier height is attributed to the improvement of hole density adjacent to the electrode as shown in the $C-V$ measurement. Besides the improvement of back-barrier height, the CdTe-CuCl devices show much shallower defect levels than the CdTe-Cu devices. In the CdTe-Cu device, two defects with depth of $E_{A2} = 0.358 \pm 0.011$ eV and $E_{A3} = 0.354 \pm 0.031$ eV are detected. While in the CdTe-CuCl devices, E_{A2} disappeared according to the change of the features in the differential capacitance spectra (Figure 4a,b), and only one defect E_{A3} =

https://doi.org/10.1021/acsami.1c11784
ACS Appl. Mater. Interfaces 2021, 13, 38432−38440

0.306 ± 0.005 eV is obtained, which is shallower than the defects in the CdTe-Cu devices. The density (N_t) and capture cross section (σ_t) of all the defects are also calculated as shown in Figure 4d and the inset. The defect E_{A3} in the CdTe-CuCl device has much lower N_t (2.69×10^{14} cm^{-3}) than that in the CdTe-Cu device (6.45×10^{14} cm^{-3} and 8.78×10^{14} cm^{-3} for E_{A2} and E_{A3}, respectively). In addition, the defects with a depth of E_{A2}, which exists in CdTe-Cu but is missing in the CdTe-CuCl device, show a much higher σ_t value of 4.83×10^{-16} cm^{-3} than the other two defects of 2.33×10^{-17} and 8.34×10^{-17} cm^{-3} for CdTe-Cu and CdTe-CuCl devices, respectively. The elimination of defects with high concentration and capture cross section in the CdTe-CuCl device can reduce the nonradiative recombination loss and improve device performance.

It is well known that Cu ions in CdTe have a high migration rate, which is the culprit of the long-term stability issue for CdTe modules. It is worth mentioning that the CuCl treatment was performed using an RTA process owing to the ionic state of CuCl, which generated a desired Cu distribution profile, i.e., a high N_{Cu} at the back surface and a low N_{Cu} at the front interface.[3] At first glance, this kind of Cu distribution profile can be double-edged, i.e., higher initial performance but lower long-term stability due to the gradient N_{Cu} profile that can promote the diffusion of Cu from the region with high N_{Cu} to the region with low N_{Cu}. To study the degradation induced by the different Cu distributions, a stability test (6 cells for each group) was carried out in ambient air for 60 days (Figure 5). For the CdTe-Cu devices, the average V_{OC} decreases by 6−7%, and the average FF decreases by 5%, yielding an average PCE relative degradation by ∼14% within 60 days. Meanwhile, the CdTe-CuCl devices show negligible degradation by ∼1 to 2%. To confirm this result, the same degradation test was also performed for another CuCl-treated device with ZMO as the front window layer instead of CdS, which shows similar stability with the CdTe-CuCl devices with CdS as the front window layer. These results further indicate that the gradient of N_{Cu} does not lead to poor stability in the CdTe-CuCl devices. The robust long-term stability performance can be attributed to the low Cu dosage in the CuCl treated devices, which results in a relatively low Cu_i concentration. Cu_i has been correlated to the fast Cu redistribution in the CdTe film and at the heterojunction, while the desired Cu_{Cd} and complexes have a relatively low diffusion rate.[36,37]

This prediction can be further demonstrated by the PL measurement at a low temperature (Figure 5d) and the SIMS measurements (Figure S5). The low-temperature PL spectra of the CdTe-Cu and CdTe-CuCl devices show similar peaks, such as a free excitonic peak at 1.59 eV,[38] a donor-acceptor pair (DAP) peak at 1.55 eV (recombination of some donor state to the V_{Cd} acceptor) and its phonon replicas,[39] and a 1.45 eV DAP peak (a DAP peak due to the recombination of Cl donor to Cu_{Cd} acceptor) and its phonon replicas at ∼20 meV.[40,41] The higher PL intensity at ∼1.45 eV in the CdTe-CuCl device is the consequence of the presence of a higher number of Cu_{Cd} acceptors at the back surface than that in the device treated with the thermally evaporated Cu. It is worth mentioning that the SIMS results suggest a lower N_{Cu} at the back surface in the CdTe-CuCl device. The low N_{Cu} and high Cu_{Cd} acceptor concentration in the CdTe-CuCl device conjointly suggest a higher formation rate of desired Cu_{Cd} substitution and a lower formation rate of compensative Cu_i, thereby enabling better long-term stability.

DISCUSSIONS

According to the device performance and characterization of the devices with different Cu precursors, the following discussions are made to understand the importance of Cu precursor in fabricating efficient CdTe solar cells.

(1) Cu diffusion. CdTe solar cells show similar performances when CuCl and $CuCl_2$ are used as the Cu precursors, with either CdS or ZMO as the front window layers. This result implies that the oxidation state of Cu in CuCl and $CuCl_2$ shows a negligible effect on the Cu incorporation. In comparison, the device with metallic Cu shows much worse device performances. These results suggest that Cu diffusion from CuCl and $CuCl_2$ into the CdTe absorber has a similar diffusion behavior and defect properties in CdTe solar cells. This is because both CuCl and $CuCl_2$ are ionic compounds and Cu ions exist naturally in these two materials; thus, no extra energy for Cu ionization is required for the Cu diffusion into CdTe. This phenomenon has recently been demonstrated in group V-doped CdTe solar cells.[42] After the diffusion into the CdTe absorber, first-principles-based analysis indicates that Cu-related defects Cu_i^+ and Cu_{Cd}^-, both of which have the Cu^+ oxidation state, have relatively low formation energies.[13,37] We assume that Cu^{2+} would change to Cu^+ and show the same diffusion rate. When metallic Cu is used as the Cu precursor, an oxidation process is needed; thus, extra energy is required to form Cu ions that can subsequently diffuse into CdTe. We suspect that this is the reason why the CuCl treatment needed lower annealing temperatures or shorter annealing duration than the metallic Cu treatment.

(2) Cu dosage and distribution. The Cu ion concentrations in both CuCl and $CuCl_2$ solutions are identical (3.10 μg/mL). Due to the difference of the CdTe layer thickness (3.5 and 4 μm for the CdS-CdTe and ZMO-CdTe, respectively), 100 μL of chloride solution is applied to 1.5″ × 1.5″ CdS-CdTe devices and 80 μL of chloride solution is applied to 1.5″ × 1.5″ ZMO-CdTe devices, which are equivalent to ∼0.24 and 0.19 Å Cu layer, respectively. Meanwhile, in the CdTe-Cu devices, the optimal Cu metal thicknesses applied in ZMO-CdTe and CdS-CdTe devices are 3 and 4 nm, respectively, which are much thicker than the equivalent Cu thickness in the CdTe-CuCl and CdTe-$CuCl_2$ devices. Nonetheless, the devices with the chloride treatment show a much higher carrier density than that with the metallic Cu treatment, suggesting that the Cu source in the chloride condition has a lower Cu dosage but a higher activation ratio (defined as the hole density relative to the incorporated dopant density) than metallic Cu.

(3) Defect properties and long-term stability. Benefiting from the low Cu dosage, the devices treated with CuCl and $CuCl_2$ possess a higher carrier density, suppressed bulk defects with shallower levels, and lower trap state capture cross section and smaller back barrier height and improved stability, simultaneously. This is because the device with a lower Cu dosage through the chloride treatment has more desired Cu_{Cd} acceptors, while the device with higher Cu dosage through metallic Cu treatment has more detrimental Cu_i donors. When the Cu dosage increases, more Cu_{Cd} will be ionized, leading to the downshift of the Fermi level toward the valence band

https://doi.org/10.1021/acsami.1c11784
ACS Appl. Mater. Interfaces 2021, 13, 38432−38440

maximum. In such a case, the formation energy of the charged donor defect Cu_i^+ (a compensating donor) decreases linearly as a function of Fermi energy, therefore, resulting in more shallow compensating Cu_i^+ donors and lower hole concentration. Due to the formation of compensating Cu_i^+ donors, the CdTe devices with thermally evaporated Cu treatment show a larger back-barrier and a more pronounced nonradiative recombination rate at the back interface. Therefore, the device performances, specifically V_{OC} and FF, are significantly limited. In addition, the formation of Cu_i^+ also introduces fast Cu ion migration throughout the CdTe film, which is the culprit of the long-term stability issue for CdTe production facilities.

(4) Effect on the devices with different front window layers. Besides the effect at the absorber bulk and device back interface, the diffusion of copper into the front interface has been widely reported in CdTe devices, which can induce deep donor defect complexes at the front interface[35,43] and decrease the n-type conductivity of the front window layer.[7,16,32,35] This effect became more notorious in CdTe solar cells with ZMO as the front window layer due to its sensitivity to Cu (with several orders of magnitude reduction of conductivity).[28−30] In the devices with CdS as the n-type window layer, the effect of Cu at the CdS-CdTe interface is weaker than that at the ZMO-CdTe interface. The solution-processed chlorine treatment successfully reduces the Cu penetration into the front interface and constructs the desired Cu distribution throughout the device; thus, the diode quality of the front main junction is improved.

CONCLUSIONS

A comparison among different Cu precursors (i.e., metallic Cu, CuCl, and $CuCl_2$ solutions) as the doping source is performed on CdTe solar cells. The similar performance of the devices with CuCl and $CuCl_2$ suggests that the oxidation states of Cu^+ and Cu^{2+} show a negligible difference on device performance. Both of them show a significant improvement in device performance compared to the devices treated with the metallic Cu. The comparison of Cu activation temperature/time, dosage, and device performance and characterization results concomitantly suggest that the solution-processed Cu treatment using a Cu ionic compound enables lower dopant diffusion and activation temperature/duration, less Cu dosage, more efficient Cu incorporation, and a desired gradient Cu profile in the CdTe film, resulting in improved electrical properties at both the front and back interfaces and the bulk of the absorber, leading to higher device performances than the conventional devices doped with metallic Cu. Finally, decent PCEs of 17.2% and 17.5% are obtained for the devices with CdS and ZMO as the front window layers, respectively, which are among the most efficient CdTe solar cells without Se incorporation.

ASSOCIATED CONTENT

Supporting Information

The Supporting Information is available free of charge at https://pubs.acs.org/doi/10.1021/acsami.1c11784.

Statistical distribution of device performance for CdS-CdTe solar cell devices with different Cu precursors; statistical distribution of device performance for ZMO-CdTe solar cell devices with different Cu precursors; EQE curves of the devices with CdS and ZMO as the window layers; *J-V* curves for the CdS-CdTe devices treated without and with HI etching treatment; secondary ion mass spectroscopy depth profiles of the CdTe-Cu and CdTe-CuCl devices with ZMO as the front window layer; post-annealing treatment for CdS-CdTe-Cu devices at 200 °C with different dwelling time; steady-state and time-resolved PL spectra of ZMO-CdTe devices with Cu metal and CuCl solution treatment; the calculated carrier densities extracted from C−V measurements for the ZMO-CdTe devices with different Cu precursors; capacitance spectra for CdTe-Cu and CdTe-CuCl devices measured under dark equilibrium (V_{DC} = 0 V) and different temperatures from 130 to 310 K with a step size of 10 K; $J-V-T$ curves for CdTe-Cu and CdTe-CuCl devices with CdS as the front window layer; Arrhenius plots extracted from the dark $J-V-T$ curves to calculate back-barrier heights (PDF)

AUTHOR INFORMATION

Corresponding Authors

Deng-Bing Li − *Department of Physics and Astronomy, and Wright Center for Photovoltaics Innovation and Commercialization (PVIC), University of Toledo, Toledo, Ohio 43606, United States;* orcid.org/0000-0003-4555-4894; Email: dengbing.li@utoledo.edu

Yanfa Yan − *Department of Physics and Astronomy, and Wright Center for Photovoltaics Innovation and Commercialization (PVIC), University of Toledo, Toledo, Ohio 43606, United States;* orcid.org/0000-0003-3977-5789; Email: yanfa.yan@utoledo.edu

Authors

Sandip S. Bista − *Department of Physics and Astronomy, and Wright Center for Photovoltaics Innovation and Commercialization (PVIC), University of Toledo, Toledo, Ohio 43606, United States;* orcid.org/0000-0003-0162-8468

Rasha A. Awni − *Department of Physics and Astronomy, and Wright Center for Photovoltaics Innovation and Commercialization (PVIC), University of Toledo, Toledo, Ohio 43606, United States*

Zhaoning Song − *Department of Physics and Astronomy, and Wright Center for Photovoltaics Innovation and Commercialization (PVIC), University of Toledo, Toledo, Ohio 43606, United States;* orcid.org/0000-0002-6677-0994

Kamala K. Subedi − *Department of Physics and Astronomy, and Wright Center for Photovoltaics Innovation and Commercialization (PVIC), University of Toledo, Toledo, Ohio 43606, United States*

Niraj Shrestha − *Department of Physics and Astronomy, and Wright Center for Photovoltaics Innovation and Commercialization (PVIC), University of Toledo, Toledo, Ohio 43606, United States;* orcid.org/0000-0001-5702-2938

Suman Rijal − *Department of Physics and Astronomy, and Wright Center for Photovoltaics Innovation and Commercialization (PVIC), University of Toledo, Toledo, Ohio 43606, United States;* orcid.org/0000-0002-7738-4917

Sabin Neupane − *Department of Physics and Astronomy, and Wright Center for Photovoltaics Innovation and*

https://doi.org/10.1021/acsami.1c11784
ACS Appl. Mater. Interfaces 2021, 13, 38432−38440

Commercialization (PVIC), University of Toledo, Toledo, Ohio 43606, United States

Corey R. Grice − *Department of Physics and Astronomy, and Wright Center for Photovoltaics Innovation and Commercialization (PVIC), University of Toledo, Toledo, Ohio 43606, United States*

Adam B Phillips − *Department of Physics and Astronomy, and Wright Center for Photovoltaics Innovation and Commercialization (PVIC), University of Toledo, Toledo, Ohio 43606, United States;* orcid.org/0000-0002-2675-5052

Randy J. Ellingson − *Department of Physics and Astronomy, and Wright Center for Photovoltaics Innovation and Commercialization (PVIC), University of Toledo, Toledo, Ohio 43606, United States;* orcid.org/0000-0001-9520-6586

Michael Heben − *Department of Physics and Astronomy, and Wright Center for Photovoltaics Innovation and Commercialization (PVIC), University of Toledo, Toledo, Ohio 43606, United States;* orcid.org/0000-0002-3788-3471

Jian V. Li − *Department of Aeronautics and Astronautics, National Cheng Kung University, 70101 Tainan, Taiwan*

Complete contact information is available at: https://pubs.acs.org/10.1021/acsami.1c11784

Author Contributions

[§]S.S.B. and D.-B.L. contributed equally. The manuscript was written through contributions of all authors. All authors have given approval to the final version of the manuscript.

Notes

The authors declare no competing financial interest.

■ ACKNOWLEDGMENTS

This work is based on research sponsored by the Air Force Research Laboratory under agreement number FA9453-18-2-0037 and FA9453-19-C-1002 and by the U.S. DOE's Office of Energy Efficiency and Renewable Energy (EERE) under Solar Energy Technologies Office (SETO) Agreement DE-EE0008974. The U.S. Government is authorized to reproduce and distribute reprints for Governmental purposes notwithstanding any copyright notation thereon. We thank Dr. David Strickler from Pilkington North America Inc. for supplying us FTO coated glass substrate. Disclaimer: The views and conclusions contained herein are those of the authors and should not be interpreted as necessarily representing the official policies or endorsements, either expressed or implied, of the U.S. Air Force Research Laboratory or the U.S. Government.

■ REFERENCES

(1) Mendis, B. G.; Ramasse, Q. M.; Shalvey, T. P.; Major, J. D.; Durose, K. Optical Properties and Dielectric Functions of Grain Boundaries and Interfaces in CdTe Thin-Film Solar Cells. *ACS Appl. Energy Mater.* **2019**, *2*, 1419−1427.

(2) Green, M. A.; Hishikawa, Y.; Dunlop, E. D.; Levi, D. H.; Hohl-Ebinger, J.; Ho-Baillie, A. W. Y. Solar Cell Efficiency Tables (version 51). *Progr. Photovolt.: Res. Appl.* **2018**, *26*, 3−12.

(3) Li, D.-B.; Bista, S. S.; Song, Z.; Awni, R. A.; Subedi, K. K.; Shrestha, N.; Pradhan, P.; Chen, L.; Bastola, E.; Grice, C. R.; Phillips, A. B.; Heben, M. J.; Ellingson, R. J.; Yan, Y. Maximize CdTe Solar Cell Performance through Copper Activation Engineering. *Nano Energy* **2020**, *73*, 104835.

(4) Ablekim, T.; Duenow, J. N.; Zheng, X.; Moutinho, H.; Moseley, J.; Perkins, C. L.; Johnston, S. W.; O'Keefe, P.; Colegrove, E.; Albin, D. S.; Reese, M. O.; Metzger, W. K. Thin-Film Solar Cells with 19% Efficiency by Thermal Evaporation of CdSe and CdTe. *ACS Energy Lett.* **2020**, *5*, 892−896.

(5) Munshi, A. H.; Kephart, J.; Abbas, A.; Raguse, J.; Beaudry, J.-N.; Barth, K.; Sites, J.; Walls, J.; Sampath, W. Polycrystalline CdSeTe/CdTe Absorber Cells with 28 mA/cm^2 Short-Circuit Current. *IEEE J. Photovolt* **2018**, *8*, 310−314.

(6) Huang, J.; Yang, D.; Li, W.; Zhang, J.; Wu, L.; Wang, W. Copassivation of Polycrystalline CdTe Absorber by CuCl Thin Films for CdTe Solar Cells. *Appl. Surf. Sci.* **2019**, *484*, 1214.

(7) Grecu, D.; Compaan, A. D. Photoluminescence Study of Cu Diffusion and Electromigration in CdTe. *Appl. Phys. Lett.* **1999**, *75*, 361−363.

(8) Krasikov, D.; Sankin, I. Defect Interactions and the Role of Complexes in the CdTe Solar Cell Absorber. *J. Mater. Chem. A* **2017**, *5*, 3503−3513.

(9) Zhang, L.; Da Silva, J. L. F.; Li, J.; Yan, Y.; Gessert, T. A.; Wei, S.-H. Effect of Copassivation of Cl and Cu on CdTe Grain Boundaries. *Phys. Rev. Lett.* **2008**, *101*, 155501.

(10) Akis, R.; Brinkman, D.; Sankin, I.; Fang, T.; Guo, D.; Vasileska, D.; Ringhofer, C. In Extracting Cu Diffusion Parameters in Polycrystalline CdTe. *IEEE 40th Photovolt Spec Conf, 8−13 June 2014*; 2014; pp. 3276−3281.

(11) Yan, Y.; Jones, K.; Zhou, J.; Wu, X.; Al-Jassim, M. TEM Study of Locations of Cu in CdTe Solar Cells. *MRS Proc.* **2011**, *1012*, 1012−Y04-09.

(12) Perrenoud, J.; Kranz, L.; Gretener, C.; Pianezzi, F.; Nishiwaki, S.; Buecheler, S.; Tiwari, A. N. A Comprehensive Picture of Cu Doping in CdTe Solar Cells. *J. Appl. Phys.* **2013**, *114*, 174505.

(13) Krasikov, D.; Knizhnik, A.; Potapkin, B.; Selezneva, S.; Sommerer, T. First-principles-based Analysis of the Influence of Cu on CdTe Electronic Properties. *Thin Solid Films* **2013**, *535*, 322−325.

(14) Paudel, N. R.; Yan, Y. Fabrication and Characterization of High-efficiency CdTe-based Thin-film Solar Cells on Commercial SnO2:F-coated Soda-lime Glass Substrates. *Thin Solid Films* **2013**, *549*, 30−35.

(15) Paudel, N. R.; Xiao, C.; Yan, Y. Close-space Sublimation Grown CdS Window Layers for CdS/CdTe Thin-film Solar Cells. *J. Mater. Sci-mater. El* **2014**, *25*, 1991−1998.

(16) Dobson, K. D.; Visoly-Fisher, I.; Hodes, G.; Cahen, D. Stability of CdTe/CdS Thin-film Solar Cells. *Sol Energy Mater. Sol Cell* **2000**, *62*, 295−325.

(17) Awni, R. A.; Li, D.-B.; Grice, C. R.; Song, Z.; Razooqi, M. A.; Phillips, A. B.; Bista, S. S.; Roland, P. J.; Alfadhili, F. K.; Ellingson, R. J.; Heben, M. J.; Li, J. V.; Yan, Y. The Effects of Hydrogen Iodide Back Surface Treatment on CdTe Solar Cells. *Solar RRL* **2019**, *3*, 1800304.

(18) Li, C.; Xu, H.; Li, K.; Ma, X.; Wu, L.; Wang, W.; Zhang, J.; Li, W.; Li, B.; Feng, L. CuTe Nanoparticles/Carbon Nanotubes as Back Contactfor CdTe Solar Cells. *J. Electron. Mater.* **2018**, *47*, 1250−1258.

(19) Wolden, C. A.; Abbas, A.; Li, J.; Diercks, D. R.; Meysing, D. M.; Ohno, T. R.; Beach, J. D.; Barnes, T. M.; Walls, J. M. The Roles of ZnTe Buffer Layers on CdTe Solar Cell Performance. *Sol. Energy Mater. Sol. Cell* **2016**, *147*, 203−210.

(20) Li, D.-B.; Bista, S. S.; Song, Z.; Alfadhili, F. K.; Awni, R. A.; Shrestha, N.; Rhiannon, D.; Phillips, A. B.; Heben, M. J.; Ellingson, R. J.; Yan, F.; Yan, Y. CuSCN as the Back Contact for Efficient ZMO/CdTe Solar Cells. *Materials* **2020**, *13*, 1991.

(21) Montgomery, A.; Guo, L.; Grice, C.; Awni, R. A.; Saurav, S.; Li, L.; Yan, Y.; Yan, F. Solution-processed Copper (I) Thiocyanate (CuSCN) for Highly Efficient CdSe/CdTe Thin-film Solar Cells. *Progr. Photovolt.: Res. Appl.* **2019**, *27*, 665−672.

(22) Artegiani, E.; Menossi, D.; Shiel, H.; Dhanak, V.; Major, J. D.; Gasparotto, A.; Sun, K.; Romeo, A. Analysis of a Novel CuCl2 Back Contact Process for Improved Stability in CdTe Solar Cells. *Progr. Photovolt.: Res. Appl.* **2019**, *27*, 706−715.

(23) Feng, X.; Singh, K.; Bhavanam, S.; Palekis, V.; Morel, D. L.; Ferekides, C. S. In Cu effects on CdS/CdTe Thin Film Solar Cells

Prepared on Flexible Substrates, *IEEE 38th Photovolt Spec Conf, 3−8 June 2012*; 2012; pp. 000843−000847.
(24) Sites, J.; Munshi, A.; Kephart, J.; Swanson, D.; Sampath, W. S. In Progress and Challenges with CdTe Cell Efficiency, *IEEE 43th Photovolt Spec Conf, 5−10 June 2016*; 2016; pp. 3632−3635.
(25) Paudel, N. R.; Grice, C. R.; Xiao, C.; Yan, Y. High Temperature CSS Processed CdTe Solar Cells on Commercial SnO2:F/SnO2 Coated Soda-lime Glass Substrates. *J. Mater. Sci-mater. El* **2015**, *26*, 4708−4715.
(26) Yang, J.; Wei, S.-H. First-principles Study of the Band Gap Tuning and Doping Control in CdSexTe1−x Alloy for High Efficiency Solar Cell. *Chin. Phys. B* **2019**, *28*, No. 086106.
(27) Li, D.-B.; Song, Z.; Awni, R. A.; Bista, S. S.; Shrestha, N.; Grice, C. R.; Chen, L.; Liyanage, G. K.; Razooqi, M. A.; Phillips, A. B.; Heben, M. J.; Ellingson, R. J.; Yan, Y. Eliminating S-Kink to Maximize the Performance of MgZnO/CdTe Solar Cells. *ACS Appl. Energy Mater.* **2019**, *2*, 2896−2903.
(28) Kutty, T. R. N.; Raghu, N. Varistors Based on Polycrystalline ZnO:Cu. *Appl. Phys. Lett.* **1989**, *54*, 1796−1798.
(29) Xu, C. X.; Sun, X. W.; Zhang, X. H.; Ke, L.; Chua, S. J. Photoluminescent Properties of Copper-doped Zinc Oxide Nanowires. *Nanotechnology* **2004**, *15*, 856−861.
(30) Hausmann, A.; Schallenberger, B.; Roll, R. A New Model for ZnO:Cu Undergoing Dynamic Jahn-Teller Coupling. *Z. Phys. B* **1980**, *40*, 1−7.
(31) Kuciauskas, D.; Dippo, P.; Zhao, Z.; Cheng, L.; Kanevce, A.; Metzger, W. K.; Gloeckler, M. Recombination Analysis in Cadmium Telluride Photovoltaic Solar Cells with Photoluminescence Spectroscopy. *IEEE J. Photovolt* **2016**, *6*, 313−318.
(32) Deng, Y.; Yang, J.; Yang, R.; Shen, K.; Wang, D.; Wang, D. Cu-doped CdS and Its Application in CdTe Thin Film Solar Cell. *AIP Adv.* **2016**, *6*, No. 015203.
(33) Awni, R. A.; Li, D.-B.; Song, Z.; Bista, S. S.; Razooqi, M. A.; Grice, C. R.; Chen, L.; Liyanage, G. K.; Li, C.; Phillips, A. B.; Heben, M. J.; Ellingson, R. J.; Li, J. V.; Yan, Y. Influences of Buffer Material and Fabrication Atmosphere on the Electrical Properties of CdTe Solar Cells. *Progr. Photovolt.: Res. Appl.* **2019**, *27*, 1115−1123.
(34) Seymour, F. H.; Kaydanov, V.; Ohno, T. R.; Albin, D. Cu and CdCl2 Influence on Defects Detected in CdTe Solar Cells with Admittance Spectroscopy. *Appl. Phys. Lett.* **2005**, *87*, 153507.
(35) Balcioglu, A.; Ahrenkiel, R. K.; Hasoon, F. Deep-level Impurities in CdTe/CdS Thin-film Solar Cells. *J. Appl. Phys.* **2000**, *88*, 7175−7178.
(36) Dzhafarov, T. D.; Yesilkaya, S. S.; Yilmaz Canli, N.; Caliskan, M. Diffusion and Influence of Cu on Properties of CdTe Thin Films and CdTe/CdS Cells. *Sol Energy Mater. Sol Cell* **2005**, *85*, 371−383.
(37) Yang, J.-H.; Yin, W.-J.; Park, J.-S.; Ma, J.; Wei, S.-H. Review on First-Principles Study of Defect Properties of CdTe as a Solar Cell Absorber. *Semicond. Sci. Technol.* **2016**, *31*, No. 083002.
(38) Liu, X.; Compaan, A. D. Photoluminescence from Ion Implanted CdTe Crystals. *MRS Online Proc. Libr.* **2005**, *865*, 525.
(39) Krustok, J.; Valdna, V.; Hjelt, K.; Collan, H. Deep Center Luminescence in P-type CdTe. *J. Appl. Phys.* **1996**, *80*, 1757−1762.
(40) Chamonal, J. P.; Molva, E.; Pautrat, J. L. Identification of Cu and Ag Acceptors in CdTe. *Solid State Commun.* **1982**, *43*, 801−805.
(41) Meyer, B. K.; Stadler, W.; Hofmann, D. M.; Omling, P.; Sinerius, D.; Benz, K. W. On the Nature of the Deep 1.4 eV Emission Bands in CdTe- A Study with Photoluminescence and ODMR Spectroscopy. *J. Cryst. Growth* **1992**, *117*, 656−659.
(42) Li, D.-B.; Yao, C.; Vijayaraghavan, S. N.; Awni, R. A.; Subedi, K. K.; Ellingson, R. J.; Li, L.; Yan, Y.; Yan, F. Low-temperature and Effective ex Situ Group V Doping for Efficient Polycrystalline CdSeTe Solar Cells. *Nat. Energy* **2021**, 715.
(43) Chin, K. K.; Gessert, T. A.; Wei, S. In The roles of CU impurity states in CdTe thin film solar cells, *IEEE 35th Photovolt Spec Conf, 20−25 June 2010*; 2010; pp. 001915−001918.

NOTE ADDED AFTER ASAP PUBLICATION

This paper was published on the Web on August 4, 2021. The title of the paper was updated, and the corrected version was reposted on August 5, 2021.

https://doi.org/10.1021/acsami.1c11784
ACS Appl. Mater. Interfaces 2021, 13, 38432−38440